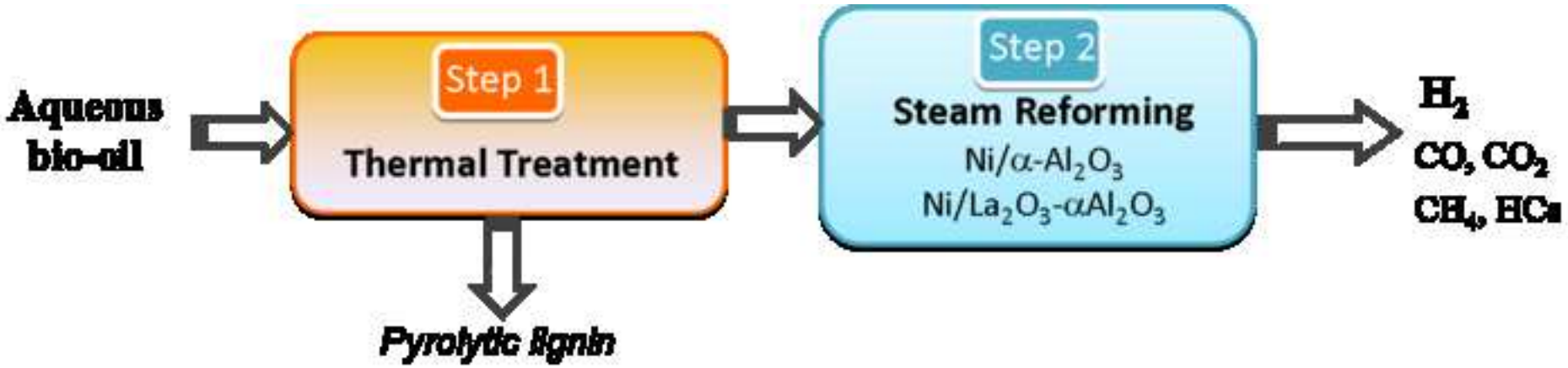

HIGHLIGHTS

- The steam reforming of bio-oil aqueous fraction in a continuous system is tackled.
- La_2O_3 addition on the Ni/αAl_2O_3 catalyst leads to higher stability an H_2 yield
- La_2O_3 enhanced WGS reaction and coke gasification.
- With Ni/La_2O_3-αAl_2O_3 complete bio-oil conversion and H_2 yield of 96 % is achieved
- Two-step reactor is effective for obtaining stable H_2 yield with continuous feed

Catalysts of Ni/α-Al_2O_3 and Ni/La_2O_3-αAl_2O_3 for hydrogen production by steam reforming of bio-oil aqueous fraction with pyrolytic lignin retention

Beatriz Valle*, Aingeru Remiro, Andrés T. Aguayo, Javier Bilbao, Ana G. Gayubo

*Chemical Engineering Department, University of the Basque Country, P. O. Box 644, 48080. Bilbao, Spain. Phone: +34 946 015361. Fax: +34 946 013 500. *Email: beatriz.valle@ehu.es*

Abstract

This paper reports on the steam reforming, in continuous regime, of the aqueous fraction of bio-oil obtained by flash pyrolysis of lignocellulosic biomass (sawdust). The reaction system is provided with two steps in series: i) thermal step at 200 ºC, for the pyrolytic lignin retention, and ii) reforming in-line of the treated bio-oil in a fluidized bed reactor, in the range 600-800 ºC, with space-time between 0.10 and 0.45 $g_{catalyst}$ h $(g_{bio\text{-}oil})^{-1}$. The benefits of incorporating La_2O_3 to the Ni/α-Al_2O_3 catalyst on the kinetic behavior (bio-oil conversion, yield and selectivity of hydrogen) and deactivation were determined. The significant role of temperature in gasifying coke precursors was also analyzed. Complete conversion of bio-oil is achieved with the Ni/La_2O_3-αAl_2O_3 catalyst, at 700 °C and space-time of 0.22 $g_{catalyst}$ h $(g_{bio\text{-}oil})^{-1}$. The catalyst deactivation is low and the hydrogen yield and selectivity achieved are 96 % and 70 %, respectively.

Keywords: hydrogen, steam reforming, bio-oil, catalyst deactivation, coke, sintering

1. Introduction

The current world consumption of hydrogen has a sustained annual growth forecast of 5-10 % (with 50 % of the total energy consumption predicted for 2100) [1,2]. In a sustainable framework, the following hydrogen market prospects can be distinguished [3]: i) large-scale industrial use, mainly for production of ammonia and methanol which is carried out currently by reforming of different petroleum fractions; ii) use in commercial sectors, such as metal processing, glass manufacture, semiconductors production (microelectronics), food industry, among others; iii) for providing heat in processes where hydrogen is generated as byproduct, such as the electrochemical obtaining of Cl and NaOH or the ethylene production by thermal craking; iv) as clean energy source or carrier with high efficiency since it posseses the highest calorific power (122 kJ/g) compared to any other known fuels. Besides, it burns cleanly, without generating any environmental pollutants and the only byproduct is water.

Currently production of hydrogen is mainly obtained from fossil fuels [4] (48 % from natural gas, 30 % from oil-derived naphtas and 18 % from coal), which results in CO_2 emissions during its production processes (mainly by steam reforming). The future hydrogen market, as fuel and energy carrier, is promoted by the need to reduce CO_2 emissions, which requires its production from renewable raw materials and energy sources. Nowotny and Veziroglu [5] predict the transition period between the petroleum based economy and that based on the hydrogen produced from renewable sources by before the year 2016.

The technological development of the different routes for hydrogen production from biomass has attracted considerable attention due to its renewable and environmentally-friendly nature [6]. Hydrogen can be generated from biomass by direct thermochemical processes (Fig. 1), such as high temperature and catalytic pyrolysis [7], gasification [8,9,], biological processes and routes with intermediate steps of production of oxygenates and their subsequent reforming [10]. The steam reforming of pyrolysis oil (bio-oil) is one of the most promising routes, based on the possibility of geographic relocation of the biomass pyrolysis plants (with simple technology, low-cost and environmentally friendly) [11] and subsequent bio-oil transportation and reforming, centralized at large-scale. However, the crude bio-oil tends to re-polymerize due to certain bio-oil components derived from the pyrolysis of the biomass lignin, which results in formation of a carbonaceous deposit (pyrolytic lignin). This deposition creates problems that affect the reactor feed system and operation, and the catalyst deactivation due to the formation of external and internal coke (within the porous structure).

Valle et el. [12] studied the nature of the coke and its location within the pores of HZSM-5 zeolite catalysts in the transformation of crude bio-oil into hydrocarbons.

Figure 1

Based on the afore-mentioned problems and with the purpose of progressing in crude bio-oil valorization, most of the studies on bio-oil reactivity and comparison of reforming catalysts have been conducted with model compounds, constituents of the complex and unstable bio-oil structure, and with bio-oil aqueous fractions. By adding water bio-oil separates into a hydrophobic lignin-derived fraction and an aqueous (hydrophilic) fraction that contains the light carbohydrate-derived compounds. Less pyrolytic lignin is deposited during the vaporization of this aqueous fraction, compared with the crude bio-oil vaporization [13].

The acetic acid reforming reaction with Ni based catalysts (promoted with La or Co) has been extensively studied in literature [14-18] as a bio-oil model compound. This type of catalysts has also been studied in reforming reactions of acetone, phenol, acetol (hydroxyacetone) [19,20], toluene [21-23], m-cresol, dibenzyl ether, glucose, xylose and sucrose [24]. Iwasa et al. [25] compared different Ni based catalysts, modified with alkali metals (Li, Na, K, Rb, Cs), in the acetic acid reforming reaction and the untreated catalyst showed the best performance. Noble metals (Pt, Pd, Rh, Ru) based catalysts, supported on α-Al_2O_3, CeO_2 and ZrO_2, have also been used for reforming reactions of acetic acid and other model compounds (acetone, phenol) [26-28].

The early studies on reforming of the aqueous fraction of bio-oil were performed in a fixed bed [29], using bio-oil fractions with high water content, which attenuates catalyst deactivation [30]. The bed blocking problems observed have been mitigated by the use of fluidized bed reactors [31-33]. Kechagiopoulos et al. [34] and Basagianis and Verykios [35] emphasized the operational difficulties due to the thermal coke deposition in the reactor walls, which led to the use of spouted bed reactors [36]. The catalysts used in those papers were based on Ni, such as commercial catalysts for naphtha reforming [29,37], Ni/Al_2O_3 modified by Ca or Mg [32], Ni/dolomite [31] and Ni/MgO [33]. Noble metals based catalysts have also been used, such as Ru-Mg-Al_2O_3 supported in monoliths, porous ceramic materials and γ-Al_2O_3 [35]. Standard hydrogen yield was 65 %, at temperature around 800 °C with S/C (steam-to-carbon ratio) greater than 10 and space velocity around WHSV = 1.0 h^{-1}. The

gasification of coke is promoted by increasing temperature and S/C and thereby the catalyst deactivation is attenuated. Yan et al. [38] studied the incorporation of CO_2 sorbents along with a commercial catalyst (not described) and they attained higher hydrogen yield with calcined dolomite (up to 83 %) and CaO (up to 85 %) than without sorbent (75 %).

In this paper, we study a continuos process with two stages in-line, thermal and catalytic, aimed at minimizing the problems inherent to lignin deposition. The first step allows a controlled pyrolytic lignin deposition and the treated bio-oil (outlet volatile stream) is reformed in the catalytic fluidized bed located in-line. Ni supported on α-Al_2O_3 catalyst (Ni/α-Al_2O_3) and other promoted with La_2O_3 (Ni/La_2O_3-αAl_2O_3) have been tested in the two-step system. This work is aimed at proving the interest of this technology, with continuous feeding of the bio-oil aqueous fraction, and these catalysts. Furthermore, the range of operating conditions more suitable for obtaining a stable and high hydrogen yield is determined.

2. Experimental

2.1. Bio-oil production and composition

Bio-oil was obtained by flash pyrolysis of pine sawdust in a semi-industrial demonstration plant, located in Ikerlan-IK4 technology center (Alava, Spain), with a biomass feeding capacity of 25 kg/h [39]. This plant was developed based on the academic results obtained in a laboratory plant (120 g/h) in the University of the Basque Country [40,41]. The aqueous fraction was obtained by phase separation after adding water to crude bio-oil, in water/bio-oil mass ratio= 2/1, by following the procedure described by Czernik et al. [37]. The composition of this aqueous fraction, in water-free basis, was determined by GC/MS analyser (*Shimadzu QP2010S device*) and it is shown in Table 1. The corresponding molecular formula is $C_{4.1}H_{7.4}O_{2.7}$.

Table 1

2.2. Catalysts

Both Ni/α-Al_2O_3 and Ni/La_2O_3-αAl_2O_3 catalysts were prepared with the method described by Alberton et al. [42]. The La_2O_3-αAl_2O_3 support was obtained by impregnation of α-Al_2O_3, under vacuum at 70 °C, with an aqueous solution of $La(NO_3)_3.6H_2O$ (*Alfa Aesar,*

99%), followed by drying at 100 °C for 24 h and calcination at 900 °C for 3 h. After the subsequent impregnation with $Ni(NO_3)_2.6H_2O$ and drying at 110 °C for 24 h, the final calcination of the catalysts was carried out at 700 °C for 3 h.

The physical properties of the catalysts (BET surface area, pore volume and average pore size) were evaluated from the N_2 adsorption-desorption isotherms, obtained by using a *Micromeritics ASAP 2010C* analyzer. This device is also used for hydrogen chemisorption measurements for quantifying metal dispersion and specific metallic surface (m^2/g_{metal}). Temperature programmed reduction (TPR) measurements were carried out for determining the reduction temperature of the different metallic phases present in the catalyst. These tests were conducted on an *AutoChem II 2920 Micromeritics*. The metal content were measured by inductively coupled plasma and atomic emission spectroscopy (ICP-AES). The X-ray diffraction (XRD) was measured on a *Bruker D8 Advance* diffractrometer with a $CuK_{\alpha 1}$ radiation.

The TPO (temperature programmed oxidation) analysis of the coke deposited on the deactivated catalysts were conducted by combustion with air in a *Setaram TG-DSC-11 Calorimeter* coupled to a mass spectrometer *Thermostar Balzers Instrument* for monitoring the signals corresponding to the masses 18 (H_2O), and 44 (CO_2).

2.3. Reaction and analysis equipment

The reaction equipment has been previously described in detail for the transformation of bio-oil and bio-oil+methanol into hydrocarbons [43] and consists of two reactors in-line (Fig. 2). The first reactor (thermal processing of bio-oil) retains the carbonaceous solid (pyrolytic lignin) formed by re-polymerization of certain bio-oil oxygenated components. The volatile compounds that leave this thermal step are subsequently transformed (by catalytic steam reforming) in the second unit (fluidized bed reactor). The controlled deposition of pyrolytic lignin in a specific thermal step, prior to the catalytic reactor, minimizes the operating problems caused by this deposition and attenuates catalyst deactivation, as has been previously verified for the catalytic conversion of crude bio-oil into hydrocarbons [44,45].

The on-line analysis of the reforming products is carried out continuously (more representative and stable than discontinuous sampling) with a gas chromatograph (*Agilent Micro GC 3000*) provided with four modules for the analysis of the following: (1) permanent gases (O_2, H_2, CO, and CH_4) with 5A molecular sieve capillary column; (2) light oxygenates

(C_{2-}), CO_2 and water, with Plot Q capillary column; (3) C_2-C_4 hydrocarbons, with alumina capillary column; (4) oxygenated compounds (C_{2+}) with Stabilwax type column.

Figure 2

2.4. Experimental conditions

The experimental two-unit system was operated at atmospheric pressure and the bio-oil aqueous fraction feeding rate (0.1 ml/min) was controlled by an injection pump *Harvard Apparatus 22*. The particle size of the catalysts was 150-250 μm and they were mixed with a solid inert (carborundum, 37 μm) in catalyst/inert mass ratio of 4/1 for improving the fluid-dynamic properties of the catalytic bed. Prior to the reforming reactions, the catalysts were reduced at 700 ºC for 2 h by using a H_2-He flow (5 vol % of H_2). The reforming conditions were: thermal step, 200 ºC; catalytic steam reforming, 600-800 ºC; steam-to-carbon ratio (steam/carbon ratio in bio-oil) at fluidized bed reactor inlet (S/C) = 12; space-time (τ) = 0.10-0.45 $g_{catalyst}$ h $(g_{bio\text{-}oil})^{-1}$; $G_{C1}HSV$= 8100-40300 h^{-1} (calculated with CH_4 equivalent units).

3. Results y discussion

3.1. Characterization of catalysts

Table 2 shows the catalytic properties, such as Ni content, BET surface area, pore volume, Ni averaged crystallite size, metallic specific surface and dispersion. BET surface of the α-Al_2O_3 support (72 m^2/g) decreases slightly with the impregnation of 10 wt% of Ni (65.5 m^2/g) and most notably with the impregnation of 10 wt% of La_2O_3 (42.5 m^2/g), due to the higher volume of the La_2O_3 molecule compared with the Ni metal. The addition of La_2O_3 to the Ni/α-Al_2O_3 catalyst does not produce a significant effect on the metallic surface and dispersion, but it involves an increase in Ni crystal size.

Table 2

Fig. 3 shows the TPR-profiles of the catalysts. The NiO reduction is observed in the range 340-600 °C [46]. The results show that the addition of La_2O_3 increases the proportion of $NiAl_2O_4$ spinel (peak at 650-676 °C) [47] due to the strong interaction between Ni and La ions, which is consistent with the findings of Sanchez-Sanchez et al. [48].

Figure 3

The XRD analysis (Fig. 4) was carried out to investigate the diffraction structure of the catalysts after reduction at 700 ºC for 2 h. Both XRD espectra are similar, with the presence of Al_2O_3 phase and Ni^0 phase, which is clearly revealed by the characteristic diffraction peaks at 2θ = 44.5º, 51.9º and 76.4º. It is also confirmed that La_2O_3 phase neither reduces nor exists in oxide form, but it combines with α-Al_2O_3 to form the $LaAlO_3$ phase.

Figure 4

3.2. Reaction indexes

Bio-oil steam reforming proceeds according to the reforming reactions of oxygenated organic compounds ($C_nH_mO_k$) and water-gas-shift reaction (WGS). The stoichiometry of the global reaction is:

$$C_nH_mO_k + (2n-k)H_2O \rightarrow nCO_2 + \left(2n + \frac{m}{2} - k\right)H_2 \quad (1)$$

The bio-oil conversion is calculated from its molar flowrates (sum of oxygenated compounds, in dry basis) at the inlet and outlet (unreacted bio-oil) of the catalytic reactor, according to:

$$X = \frac{F_{\text{bio-oil,inlet}} - F_{\text{bio-oil,outlet}}}{F_{\text{bio-oil,inlet}}} \quad (2)$$

The hydrogen yield is calculated as a percentage of the stoichiometric potential, in case of complete conversion of the carbon contained in bio-oil to CO_2 (according to the Eq. (1)):

$$Y_{H_2} = \frac{\text{molar flow of } H_2 \text{ obtained}}{(2n + m/2 - k) \times \text{molar flow of C in the feed}/n} \times 100 \quad (3)$$

The yield of each carbon-containing byproduct (CO, CO_2, CH_4 and light hydrocarbons C_2-C_4) is quantified by:

$$Y_i = \frac{\text{moles of i } (CO, CO_2, CH_4, HCs) \text{ obtained}}{\text{moles of C in the feed}} \times 100 \quad (4)$$

The selectivity of each *i* product is calculated:

$$S_i = \frac{\text{molar flow of i obtained}}{\text{molar flow of C in the feed}} \times 100 \quad (5)$$

3.3. Effect of La_2O_3 addition to Ni/α-Al_2O_3 catalyst

Two parameters that have an important effect on hydrogen yield (reaction temperature and space-time) were investigated with Ni/α-Al_2O_3 and Ni/La_2O_3-αAl_2O_3 catalysts. The thermal treatment (first step at 200 °C) of the aqueous bio-oil ($C_{4.1}H_{7.4}O_{2.7}$) retained 30 wt% of pyrolytic lignin (referred to bio-oil oxygenates). Consequently, the composition of the treated bio-oil that enters the fluidized bed reactor is $C_{3.7}H_{8.4}O_{2.9}$ and thus the maximum yield (stoichiometric) of hydrogen is 2.35 moles H_2/mol C fed.

Fig. 5 shows the effect of reaction temperature on bio-oil conversion (Fig. 5a) and hydrogen yield (Fig. 5b) with time on stream. Table 3 shows the results of hydrogen selectivity and the yields of CO, CO_2, CH_4 and hydrocarbons, corresponding to the fresh catalyst (t = 0 h) and after 5 h of reaction.

The space-time used in these experiments (0.22 $g_{catalyst}$ h $(g_{bio\text{-}oil})^{-1}$) is enough for attaining complete conversion at zero time on stream (fresh catalyst) for both catalysts and, consequently, no remarkable effect of temperature on bio-oil initial conversion is observed. However, the reaction temperature has a significant effect on the evolution with time on stream of bio-oil conversion due to its effect on the catalysts deactivation (studied in following sections). Fig. 5a shows that deactivation is attenuated with the increase in temperature from 600 ºC up to 700 ºC. When this exceeds 700 ºC, bio-oil conversion is almost constant for 5 h of reaction. Furthermore, the addition of La_2O_3 to the catalyst does not have a notable effect on bio-oil conversion at 600 °C (when the deactivation is pronounced for both catalysts).

As shown in Fig. 5b, the hydrogen yield at zero time on stream is almost independent of temperature for both catalysts. However, the temperature has a noticeable effect on deactivation and a rapid decrease in hydrogen yield with time on stream is observed at 600 °C. This effect is attenuated when reaction temperature is above 700 ºC. The deactivation observed at 800 ºC is higher than at 700 °C, especially with the Ni/α-Al_2O_3 catalyst because of the nickel sintering (discussed below). It is noteworthy that hydrogen production is higher with the Ni/La_2O_3-αAl_2O_3 catalyst for the three temperatures studied. This favourable effect of La_2O_3 incorporation may be attributed to its water adsorption capacity [49] thereby favouring the WGS reaction, for which the Ni/α-Al_2O_3 catalyst has moderate activity [50,51].

Figure 5

In Table 3 the results of hydrogen selectivity and the yields of byproducts (CO_2, CO, CH_4 and C_{2+} hydrocarbons) at zero time on stream and at 5 h of time on stream are set out. Initial hydrogen selectivity is maximum at 700 °C for the Ni/α-Al_2O_3 catalyst (69.6 %) and at 600 °C for the Ni/La_2O_3-αAl_2O_3 catalyst (71.2 %). After 5 h of time on stream this selectivity achieved a maximum at 600 ºC for both catalysts due to deactivation. The increase in CO yield with time on stream is consequence of the catalysts deactivation, which affects the catalytic steam reforming and WGS reactions. Moreover, thermal decomposition reactions of bio-oil oxygenated compounds are enhanced by the catalyst deactivation, with the consequent formation of CO, CH_4 and hydrocarbons. The results of Fig. 5 and Table 3 emphasize that the addition of La_2O_3 to the catalyst significantly reduces deactivation and thus attenuates the formation of these byproducts.

Table 3

Fig. 6 shows the effect of space-time on the evolution with time on stream of bio-oil conversion (Fig. 6a) and hydrogen yield (Figure 6b) for both catalysts at 700 ºC. Table 4 shows the values of hydrogen selectivity and byproducts yields corresponding to the fresh catalyst (t = 0 h) and after 5 h of time on stream.

Figure 6

Table 4

In the space-time range studied (0.10-0.45 $g_{catalyst}$ h $(g_{bio\text{-}oil})^{-1}$) the Ni/$La_2O_3$-α$Al_2O_3$ catalyst shows a better performance (higher bio-oil conversion and hydrogen yield and lower deactivation) than the Ni/α-Al_2O_3. A space-time around 0.45 $g_{catalyst}$ h $(g_{bio\text{-}oil})^{-1}$ is necessary for attaining complete conversion over the Ni/α-Al_2O_3 catalyst (which remains almost constant for 5 h (Fig. 6a)) and hydrogen yield near to the stoichiometric value (which decreases slightly with time on stream (Fig. 6b)). These targets are achieved for a space-time of 0.22 $g_{catalyst}$ h $(g_{bio\text{-}oil})^{-1}$ with the Ni/La_2O_3-αAl_2O_3 catalyst. For both catalysts, the increase in space-time contributes to attenuating deactivation. As shown in Table 4, an increase in space-time causes a slight increase in the initial values of hydrogen selectivity and CO_2 yield and a decrease in the yields of CO, CH_4 and hydrocarbons. After 5 h of reaction (when catalyst is partially deactivated and thus conversion is far from being complete) the space-

time effect is more significant.

The increase in CO yield with time on stream due to WGS reaction deactivation and thermal decomposition reactions of bio-oil oxygenates is greatly attenuated by the addition of La_2O_3, and thereby half the space-time is enough for obtaining the same hydrogen yield. The CH_4 yield, which has great influence on hydrogen yield (as it has 4 H atoms per molecule), follows the same trend with reaction time and space-time as the CO yield. The addition of La_2O_3 also helps to reduce the formation of CH_4 and light hydrocarbons.

3.4. Stability and deactivation of Ni/La_2O_3-αAl_2O_3 catalyst

The catalysts stability was tested in long-term reactions (20 h) and the results of bio-oil conversion and hydrogen yield and selectivity are shown in Fig. 7. Bio-oil conversion (Fig. 7a) decreases from 100 % to 96 % for 20 h of time on stream with the Ni/α-Al_2O_3 catalyst, while the hydrogen yield (Fig. 7b) gradually dropped from 94 % to 65 % that indicates notable deactivation of the catalyst. The Ni/La_2O_3-αAl_2O_3 catalyst is more stable, with almost constant conversion around 100 %. The hydrogen yield decreases from 95 % to 85 % and the selectivity from 70 % to 66 %.

Figure 7

The above results confirm that La_2O_3 provides stability to the Ni/α-Al_2O_3 catalyst, thereby attenuating significantly its deactivation. Possible causes are: i) La_2O_3 capacity for water adsorption [49,51], which favours the WGS reaction and inhibits the adsorption of coke precursors and their growth mechanism (oligomerization-aromatization-condensation reactions); ii) the increase in the amount of surface oxygen in metal sites due to the creation of oxygen vacancy defects that promoting the migration of O^{2-} ions on the Ni metallic surface by the lower valence of La^{3+} [52]. Furthermore, certain authors [51,53-55] reported the La_2O_3 capacity for generating surface oxygen by the formation of $La_2O_2CO_3$ carbonate, which is active for reacting with the coke and thus cleaning the Ni metallic surface; iii) the basic character of La_2O_3 may neutralize the low acidity of α-Al_2O_3, and therefore attenuate hydrocarbon formation (by dehydration) and their evolution to coke precursors. Certain authors emphasize the role of La_2O_3 and attribute coke formation to the degradation of the hydrocarbons formed by secondary reactions in the steam reforming [56]. In addition, La_2O_3 provides thermal stability to the catalyst, attenuating the formation of Ni atom clusters [57].

Temperature programmed oxidation (TPO) curves of the coke deposited on both catalysts after 5 h of time on stream, at 700 ºC and space-time 0.45 $g_{catalyst}$ $h/g_{bio\text{-}oil}^{-1}$, are shown in Figure 8. These results correspond to the incipient coke deposition, with very low contents of 0.25 wt% for the Ni/α-Al_2O_3 catalyst and 0.11 wt% for the Ni/La_2O_3-αAl_2O_3 catalyst. Three peaks can be distinguished: the first one around 275 °C for both catalysts; the second one at 420 ºC, only detected over the Ni/α-Al_2O_3 catalyst, and the third peak, detected at 660 °C for the Ni/α-Al_2O_3 catalyst and shifted slightly to lower temperature for the Ni/La_2O_3-αAl_2O_3 catalyst.

Figure 8

The three peaks observed in the TPO curves may be attributed to: i) coke deposited on Ni metal particles (the peak at lower temperature), which is easily accessible to gasification during the steam reforming and to oxygen during its combustion, activated by these Ni particles; ii) coke presumably deposited on the Ni-La_2O_3 and/or Ni-Al_2O_3 interface, whose gasification is enhanced by La_2O_3 and thus it is negligible for the Ni/La_2O_3-αAl_2O_3 catalyst above 700 °C and high values of space-time; iii) coke deposited on the α-Al_2O_3 support, whose combustion is not catalytically actived and may even be hindered by the oxygen diffusional limitation within the porous structure of this α-Al_2O_3. These hypothesis are supported by studies in literature that highlight the interest of studing the TPO profiles to analyze the coke nature and its location for different catalytic processes [12,58-61]. The magnitude and position of these peaks depend on both the catalyst and operating conditions and, therefore, the determination of the nature and location of the different types of coke require further studies, which are out of the scope of this paper.

Table 5 shows the results of coke content deposited over both catalysts at 600, 700 and 800 °C, at space-time value of 0.22 $g_{catalyst}$ $h/g_{bio\text{-}oil}$. The results listed in Table 6 correspond to different values of space-time (0.1, 0.22 and 0.45 $g_{catalyst}$ $h/g_{bio\text{-}oil}^{-1}$) at 700 °C.

Table 5

Table 6

Coke contents decreases with the increase in temperature (Table 5) and space-time (Table 6) for both catalysts, which is consistent with the afore-mentioned effect of these variables on the reaction indexes evolution with time on stream. It is also noteworthy that

La_2O_3 addition helps to reduce the coke content and the second peak is hardly observed in the TPO profile for both catalysts at low coke contents.

Based on the above results, the amount of coke that deposits over Ni particles is greatly attenuated by the La_2O_3 addition, since this disfavors its formation and promotes gasification [49,53-55]. Furthermore, this gasification is favoured by increasing temperature (Table 5) and space-time (Table 6). The temperature increase has the opposite effects of enhancing coke formation mechanisms [62] and promoting its gasification, which results in a very low amount of coke deposited at 700 °C.

In addition to coke deposition, other possible cause of catalyst deactivation is the sintering of Ni metal particles, in whose mechanism the reaction temperature has a significant effect. Table 7 shows the results of the average Ni particle size, determined by XRD for both catalysts, fresh and deactivated (after 5 h of reaction) at 700 ºC. The largest Ni particle diameter observed in the fresh catalyst promoted with La_2O_3 has also been observed previously [57,63] for lower La_2O_3 contents. The catalyst without La_2O_3 undergoes sintering at 700 °C, thereby doubling its initial Ni particle size and reducing the metal surface available for reactants adsorption, which results in low reforming activity. The addition of La_2O_3 avoids sintering, by separating the Ni crystals and thus favoring their reducibility and attenuating the formation of clusters [63]. This temperature limit of 700 °C for avoiding the sintering of Ni supported on Al_2O_3 has also been observed by Ibrahim and Idem [64] in the reforming of gasoline with partial oxidation.

Table 7

It is worth pointing out that catalyst deactivation by sintering reduces the reforming and WGS reactions rates and it also has the secondary effect of promoting the undesirable reactions of bio-oil thermal decomposition, which lead to formation of byproducts (CO, CH_4 and hydrocarbons). The hydrocarbons formed may condense to form more coke over the Ni metal particles. This secondary effect helps to justify the afore-mentioned rapid deterioration of reaction indexes at 800 °C.

4. Conclusions

The proposed reaction equipment is suitable for continuous reforming of the aqueous fraction of bio-oil, without operational problems and with low catalyst deactivation, when

working under suitable conditions. The process consists of two stages in series; the first one at 200 °C for the pyrolytic lignin retention, and the second one (fluidized bed reactor) for in-line catalytic reforming of the treated bio-oil.

The results obtained at different values of reforming temperature and space-time show that La_2O_3 addition to the Ni/α-Al_2O_3 catalyst improves the hydrogen yield and selectivity. The deactivation is also significantly attenuated by the enhanced water adsorption capacity, which is a key stage for steam reforming of oxygenates adsorbed in Ni particles.

The gasification of coke precursors are enhanced by the increase in reaction temperature above 700 °C and, in a lesser extent, by the increase in space-time. At this temperature, gasification is more favored than the formation of coke precursors by the degradation of bio-oil oxygenates. The Ni/La_2O_3-αAl_2O_3 catalyst dos not undergo deactivation by sintering at 700 ºC due to the La_2O_3 addition and complete conversion of bio-oil is achieved, at space-time of 0.22 $g_{catalyst}$ h $(g_{bio\text{-}oil})^{-1}$, with hydrogen yield of 96 % and 70 % of hydrogen selectivity.

It is concluded that continuous reforming of the aqueous fraction of bio-oil is feasible in the two-step reaction system used and over these catalysts. These results are hopeful to face in future research works, the study of crude bio-oil reforming with this technology and the Ni/La_2O_3-αAl_2O_3 catalyst.

Acknowledgments

This work was carried out with the financial support of the Department of Education Universities and Investigation of the Basque Government (Project GIC07/24-IT-220-07), of the University of the Basque Country (UFI 11/39) and of the Ministry of Science and Innovation of the Spanish Government (Project CTQ2009-13428/PPQ).

Nomenclature

C_C	Coke content, wt %
d_M	Average diameter of Ni metal particle, nm
$F_{bio\text{-}oil,}$	Molar flow rate of bio-oil, in dry basis, mol h^{-1}
$G_{C1}HSV$	Gas hourly space velocity, defined in equivalent CH_4 units, h^{-1}
Y_{H2}	Hydrogen yield for the reforming step, expressed as percentage of the stoichiometric maximum, %
Y_i	*i* carbonaceous product yield, in units of carbon fed, mol *i* (mol C fed)$^{-1}$, %
S/C	Steam to (carbon in the bio-oil) ratio fed to the reactor
S_{BET}	BET surface area, $m^2\ g^{-1}$
S_m	Specific metal surface, $m^2\ g_{metal}^{-1}$
S_{H2}	Hydrogen selectivity, %
T	Temperature, ^oC.
V_{pore}	Pore volume, cm^3g^{-1}
X	Bio-oil conversion
τ	Space-time, $g_{catalyst}\ h\ (g_{bio\text{-}oil})^{-1}$

References

[1] Demirbas A. Biohydrogen for future engine fuel demands. Springer. 2009. London.

[2] Kirtay E. Recent advances in production of hydrogen from biomass. Energy Conver. Manage. 2011; 52:1778.

[3] Levin DB, Chahine R. Challenges for renewable hydrogen production from biomass. Int. J. Hydrogen Energy. 2010; 35:4962.

[4] Balat H, Kirtay E. Hydrogen from biomass-Present scenario and future prospects. Int. J. Hydrogen Energy. 2010; 35:7416.

[5] Nowotny J, Veziroglu TN. Impact of hydrogen on the environment. Int. J. Hydrogen Energy. 2011; 36:13218.

[6] Kalinci Y, Hepbasli A, Dincer I. Biomass-based hydrogen production: A review and analysis. Int. J. Hydrogen Energy. 2009; 34:8799.

[7] Qinglan H, Chang W, Dingqiang LY, Dan L, Guiju L. Production of hydrogen-rich gas from plant biomass by catalytic pyrolysis at low temperature. Int. J. Hydrogen Energy. 2010; 35:8884.

[8] Yoon HC, Cooper T, Steinfeld A. Non-catalytic autothermal gasification of woody biomass. Int. J. Hydrogen Energy. 2011; 36:7852.

[9] Acharya B, Dutta A, Basu P. An investigation into steam gasification of biomass for hydrogen enriched gas production in presence of CaO. Int. J. Hydrogen Energy. 2010; 35, 1582.

[10] Holladay JD, Hu J, King DL, Wang Y. An overview of hydrogen production technologies. Catal. Today. 2009; 139:244.

[11] Butler E, Devlin G, Meier D, McDonnell K. A review of recent laboratory research and commercial developments in fast pyrolysis and upgrading. Renew. Sust. Energy Rev. 2011; 15:4171.

[12] Valle B, Castaño P, Olazar M, Bilbao J, Gayubo AG. Deactivating species in the transformation of crude bio-oil with methanol into hydrocarbons on a HZSM-5 catalyst. J. Catal. 2012; 285:304.

[13] Gayubo AG, Aguayo AT, Atutxa A, Prieto R, Bilbao J. Deactivation of a HZSM-5 catalyst in the transformation of the aqueous fraction of biomass pyrolysis-oil into hydrocarbons. Energy Fuels. 2004; 18:1640.

[14] Wang D, Czernik S, Montané D, Mann M, Chornet E. Biomass to hydrogen via fast pyrolysis and catalytic steam reforming of the pyrolysis oil or its fractions. Ind. Eng. Chem. Res. 1997; 36:1507.

[15] Galdámez JR, García L, Bilbao R. Hydrogen production by steam reforming of bio-oil using co-precipited NiAl catalysts. Acetic acid as a model compound. Energy Fuels. 2005; 19:1133.

[16] Basagianis AC, Verykios XE. Reforming reactions of acetic acid on nickel catalysts over a wide temperature range. Appl. Catal. A: General. 2006; 308:182.

[17] Bimbela F, Oliva M, Ruiz J, García L, Arauzo J. Hydrogen production by catalytic steam reforming of acetic acid, a model compound of biomass pyrolysis liquids. J. Anal. Appl. Pyrolysis. 2007; 79:112.

[18] Medrano JA, Oliva M, Ruiz J, García L, Arauzo J. Catalytic steam reforming of acetic acid in a fluidized bed reactor with oxygen addition. Int. J. Hydrogen Energy. 2009; 34:7064.

[19] Bimbela F, Oliva M, Ruiz J, García L, Arauzo J. Catalytic steam reforming of model compounds of biomass pyrolysis liquids in fixed bed: acetol and n-butanol. J. Anal. Appl. Pyrolysis. 2009; 85:204.

[20] Ramos MC, Navascués AI, García L, Bilbao R. Hydrogen production by catalytic steam reforming of acetol, a model compound of bio-oil. Ind. Eng. Chem. Res. 2007; 46:2399.

[21] Bona S, Guillén P, Alcalde JG, García L, Bilbao R. Toluene steam reforming using coprecipited Ni/Al catalysts modified with lanthanum or cobalt. Chem. Eng. J. 2008; 137:587.

[22] Yoon SJ, Cho YC, Lee JG. Hydrogen production from biomass tar by catalytic steam reforming. Energy Convers. Manage. 2010; 51:42.

[23] Zhao B, Zhang X, Chen L, Qu R, Meng G, Yi X, Sun L. Steam reforming of toluene as model compound of biomass pyrolysis tar for hydrogen. Biomass Bioenergy. 2010; 34:140.

[24] Marquevich M, Czernik S, Chornet E, Montané D. Hydrogen from biomass: Steam reforming of model compounds of fast-pyrolysis oil. Energy Fuels. 1999; 13:1160.

[25] Iwasa N, Yamane T, Arai M. Influence of alkali metal modification and reaction conditions on the catalytic activity and stability of Ni containing smectite-type material for steam reforming of acetic acid. Int. J. Hydrogen Energy. 2011; 36:5904.

[26] Rioche C, Kulkarni S, Meunier FC, Breen JP, Burch R. Steam reforming of model compounds and fast pyrolysis bio-oil on supported noble metal catalysts. Appl. Catal. B: Environmental. 2005; 61:130.

[27] Takanabe K, Aika K, Inazu K, Baba T, Seshan K, Lefferts L. Steam reforming of acetic acid as a biomass derived oxygenate: Bifunctional pathway for hydrogen formation over Pt/ZrO_2 catalysts. J. Catal. 2006; 243:263.

[28] Takanabe K, Aika K, Seshan K, Lefferts L. Catalyst deactivation during steam reforming of acetic acid over Pt/ZrO_2. Chem. Eng. J. 2006; 120:133.

[29] Wang D, Czernik S, Chornet E. Production of hydrogen from biomass by catalytic steam reforming of fast pyrolysis oils. Energy Fuels. 1998; 12:19.

[30] Chen T, Wu C, Liu R. Steam reforming of bio-oil from rice husks fast pyrolysis for hydrogen production. Bioresour. Technol. 2011; 102:9236.

[31] Li H, Xu Q, Xue H, Yan Y. Catalytic reforming of the aqueous phase derived from fast-pyrolysis of biomass. Renew. Energy. 2009; 34:2872.

[32] Medrano JA, Oliva M, Ruiz J, García L, Arauzo J. Hydrogen from aqueous fraction of biomass pyrolysis liquids by catalytic steam reforming in fluidized bed. Energy. 2011; 36:2215.

[33] Zhang S, Li X, Xu Q, Yan Y. Hydrogen production from the aqueous phase derived from fast pyrolysis of biomass. J. Anal. Appl. Pyrolysis. 2011; 92:158.

[34] Kechagiopoulos PN, Voutetakis SS, Lemonidou AA, Vasalos IA. Hydrogen production via reforming of the aqueous phase of bio-oil in a fixed bed reactor. Energy Fuels. 2006; 20:2155.

[35] Basagianis AC, Verykios XE. Steam reforming of the aqueous fraction of bio-oil over structured $Ru/MgO/Al_2O_3$ catalysts. Catal. Today. 2007; 127:256.

[36] Kechagiopoulos PN, Voutetakis SS, Lemonidou AA, Vasalos IA. Hydrogen production via reforming of the aqueous phase of bio-oil over Ni/olivine catalysts in a spouted bed reactor. Ind. Eng. Chem. Res. 2009; 48:1400.

[37] Czernik S, French R, Feik C, Chornet E. Hydrogen by catalytic steam reforming of liquid byproducts from biomass thermoconversion processes. Ind. Eng. Chem. Res. 2002; 41:4209.

[38] Yan CF, Hu EY, Cai CL. Hydrogen production from bio-oil aqueous fraction with in situ carbon dioxide capture. Int. J. Hydrogen Energy. 2010; 35:2612.

[39] Makibar J, Fernandez-Akarregi AR, Alava I, Cueva F, Lopez G, Olazar M. Investigations on heat transfer and hydrodynamics under pyrolysis conditions of a pilot-plant draft tube conical spouted bed reactor. Chem. Eng. Process.: Process Inten. 2012; 50:790.

[40] Amutio M, López G, Artetxe M, Elordi G, Olazar M, Bilbao J. Influence of temperature on biomass pyrolysis in a conical spouted bed reactor. Resour. Conserv. Recycling. 2012; 59:23.

[41] Amutio M, Lopez G, Aguado R, Bilbao J, Olazar M. Biomass oxidative flash pyrolysis: autothermal operation, yields and product properties. Energy Fuels. 2012; 26:1353.

[42] Alberton AL, Souza MMVM, Schmal M. Carbon formation and its influence on ethanol steam reforming over Ni/Al_2O_3 catalysts. Catal. Today. 2007; 123:257.

[43] Gayubo AG, Valle B, Aguayo AT, Olazar M, Bilbao J. Pyrolytic lignin removal for the valorisation of biomass pyrolysis crude bio-oil by catalytic transformation. J. Chem. Tech. Biotechnol. 2010; 85:132.

[44] Gayubo AG, Valle B, Aguayo AT, Olazar M, Bilbao J. Olefin production by catalytic transformation of crude bio-oil in a two-step process. Ind. Eng. Chem. Res. 2010; 49:123.

[45] Valle B, Gayubo AG, Aguayo AT, Olazar M, Bilbao J. Selective production of aromatics by crude bio-oil valorization with a Ni modified HZSM-5 catalyst. Energy Fuels. 2010; 24:2060.

[46] Akande AJ, Idem RO, Dalai AK. Synthesis, characterization and performance evaluation of Ni/Al_2O_3 catalysts for reforming of crude ethanol for hydrogen production. Appl. Catal. A: General. 2005; 287:159

[47] Li C, Chen YW. Temperature-programmed-reduction studies of nickel oxide/alumina catalysts: effects of the preparation method. Thermochim. Acta. 1995; 256:457.

[48] Sánchez-Sánchez MC, Navarro RM, Fierro JLG. Ethanol steam reforming over Ni/La-Al_2O_3 catalysts: Influence of lanthanum loading. Catal. Today. 2007; 129:336.

[49] Garcia L, French R, Czernik S, Chornet E. Catalytic steam reforming of bio-oils for the production of hydrogen: Effects of catalyst composition. Appl. Catal. A: General.2000; 201:225.

[50] Zhang L, Li W, Liu J, Guo C, Wang Y, Zhang J. Ethanol steam reforming over Al_2O_3.SiO_2-supported Ni-La catalysts. Fuel. 2009; 88:511.

[51] Chowdhury MBI, Hossain MM, Charpentier PA. Effect of supercritical water gasification treatment on Ni/La_2O_3-Al_2O_3-based catalysts. Appl. Catal. A: General. 2001; 405:84.

[52] López-Haro M, Aboussaíd K, González JC, Hernández JC, Pintado JM, Blanco G, Calvino JL, Midgley PA, Bayle-Guillemaud P, Trasobares S. Scanning transmission electron microscopy investigation of differences in the high temperatura redox deactivation behavior of $CePrO_x$ particles supported on modified alumina. Chem. Mater. 2009; 21:1035.

[53] Fatsikostas AN, Kondarides DI, Verykios XE. Production of hydrogen for fuel cells by reformation of biomass-derived ethanol. Catal. Today. 2002; 75:145.

[54] Yung MM, Jablonski WS, Magrini-Bair KA. Review of catalytic conditioning of biomass derived syngas. Energy Fuels. 2009; 23:1874.

[55] Serrano-Lotina A, Rodríguez L, Muñoz G, Martin AJ, Folgado MA, Daza L. Biogas reforming over La-NiMgAl catalysts derived from hydrotalcite-like structure: Influence of calcination temperature. Catal. Commun. 2011; 12:961.

[56] Verykios XE. Catalytic dry reforming of natural gas for the production of chemicals and hydrogen. Int. J. Hydrogen Energy. 2003; 28:1045.

[57] Kumar P, Sun Y, Idem RO. Comparative study of Ni-based mixed oxide catalyst for carbon dioxide reforming of methane. Energy Fuels. 2008; 22:3575.

[58] Sierra I, Ereña J, Aguayo AT, Olazar M, Bilbao J. Regeneration of CuO-ZnO-Al_2O_3/γ-Al_2O_3 catalyst in the direct synthesis of dimethyl ether. Appl. Catal. B: Environmental. 2010; 94:108.

[59] Castaño P, Elordi G, Olazar M, Aguayo AT, Pawelec BG, Bilbao J. Insights into the coke deposited on HZSM-5, Hβ and HY zeolites during the cracking of polyethylene. Appl. Catal B: Environmental. 2011; 104:91.

[60] Castaño P, Gutiérrez A, Hita I, Arandes JM, Aguayo AT, Bilbao J. Deactivating species deposited on Pt-Pd catalysts in the hydrocracking of light cycle oil. Energy Fuels. 2012; 26:1509.

[61] Ereña J, Sierra I, Olazar M, Gayubo AG, Aguayo AT. Deactivation of a CuO-ZnO-Al_2O_3/gamma-Al_2O_3 catalyst in the synthesis of dimethyl ether. Ind. Eng. Chem. Res. 2008; 47:2238.

[62] Bartholomew, C.H., Mechanisms of catalyst deactivation, *App. Catal. A: General*, 212 (2001) 17-60.

[63] Bang Y, Seo JG, Song IK. Hydrogen production by steam reforming of liquefied natural gas (LNG) over mesoporous Ni-La-Al_2O_3 aerogel catalyts: Effect of La content. Int. J. Hydrogen Energy. 2011; 36:8307.

[64] Ibrahim HH, Idem RO. Single and mixed oxide-supported nickel catalysts for the catalytic partial oxidation reforming of gasoline. Energy Fuels. 2008; 22:878.

Figure Captions

Figure 1. Routes for obtaining hydrogen from biomass.

Figure 2. Scheme of reaction equipment.

Figure 3. Temperature programmed reduction (TPR) profiles of the catalysts.

Figure 4. XRD spectra for catalysts (reduced by 5 vol% H_2 at 700 ºC for 2 h).

Figure 5. Effect of temperature on the evolution with time on stream of bio-oil conversion (a) and (b) H_2 yield, for Ni/α-Al_2O_3 and Ni/La_2O_3-αAl_2O_3 catalysts. Conditions: 600 ºC (G_{C1}HSV = 14500 h^{-1}), 700 ºC (G_{C1}HSV = 16100 h^{-1}), 800 ºC (G_{C1}HSV = 17800 h^{-1}), S/C = 12, τ = 0.22 $g_{catalyst}h(g_{bio\text{-}oil})^{-1}$.

Figure 6. Effect of space-time on the evolution with time on stream of bio-oil conversion (a) and H_2 yield (b), for Ni/α-Al_2O_3 and Ni/La_2O_3-αAl_2O_3 catalysts. Conditions: 700 ºC, S/C = 12.

Figure 7. Evolution with the time on stream of bio-oil conversion (a) and H_2 yield and selectivity (b), for Ni/α-Al_2O_3 and Ni/La_2O_3-αAl_2O_3 catalysts. Conditions: 700 ºC, G_{C1}HSV = 8100 h^{-1}, S/C = 12, τ = 0.45 $g_{catalyst}h(g_{bio\text{-}oil})^{-1}$.

Figure 8. Comparison of TPO profiles for both catalysts, under conditions of incipient coke deposition. Conditions: 700 ºC, S/C = 12, G_{C1}HSV = 8100 h^{-1}, t = 5 h, τ = 0.45 $g_{catalyst}h(g_{bio\text{-}oil})^{-1}$.

TABLES

Table 1. Mass composition and molecular formula of the aqueous fraction of the bio-oil used.

Compound	wt %
Acetic acid	19.1
Acetone	1.0
Formic acid	2.7
Methanol	1.0
1-hydroxy-2-propanone	8.7
Hydroxyacetaldehyde	1.8
1-hydroxy-2-butanone	2.0
Levoglucosane	19.6
Hexose	2.7
Other ketones	6.1
Other acids	4.7
Esters	3.1
Other aldehydes	5.5
Phenols	13.4
Ethers	0.3
Alcohols	3.6
Others	1.1
Unidentified	3.8
Molecular formula	$C_{4.1}H_{7.4}O_{2.7}$

Table 2. Properties of the catalysts.

Catalyst	Metal content wt %	S_{BET} m^2/g	V_{pore} cm^3/g	d_M nm	S_m m^2/g_{metal}	Ni dispersion %
αAl_2O_3	-	72.0	0.210	-	-	-
La_2O_3-αAl_2O_3	5.03 ± 2.08 (La_2O_3)	42.4	0.170	-	-	-
Ni/αAl_2O_3	8.93 ± 0.03 (Ni)	65.5	0.174	7.4	14.1	2.1
Ni/La_2O_3-αAl_2O_3	9.92 ± 1.07 (Ni)	37.6	0.145	11.9	12.4	1.9

Table 3. Effect of temperature on H_2 selectivity and on yields of CO_2, CO, CH_4 and hydrocarbons at zero time on stream (fresh catalyst) and at 5 h time on stream for Ni/α-Al_2O_3 and Ni/La_2O_3-αAl_2O_3 catalysts.

Catalyst	T, °C	t, h	S_{H2}, %	Y_{CO2}, %	Y_{CO}, %	Y_{CH4}, %	Y_{HCs}, %
Ni/α-Al_2O_3	600	0	68.6	93.9	6.3	0.2	0
		5	65.5	66.8	16.1	1.3	0.3
	700	0	69.6	90.3	8.6	0.3	0
		5	63.5	73.0	23.3	3.0	0.5
	800	0	68.8	85.5	15.0	0.6	0
		5	61.3	66.8	27.1	6.5	0.6
Ni/La_2O_3-αAl_2O_3	600	0	71.2	93.6	6.0	0.3	0
		5	69.1	77.3	11.4	1.0	0.3
	700	0	69.5	89.0	9.2	0.3	0
		5	68.3	84.3	10.8	0.9	0.2
	800	0	70.3	84.9	12.6	0.5	0
		5	64.9	77.7	18.0	4.8	0.4

Table 4. Effect of space time on H_2 selectivity and on yields of CO_2, CO, CH_4 and hydrocarbons at zero time on stream (fresh catalyst) and at 5 h time on stream for Ni/α-Al_2O_3 and Ni/La_2O_3-αAl_2O_3.

Catalyst	τ, g_{cat} h/$g_{bio\text{-}oil}$	t, h	S_{H2}, %	Y_{CO2}, %	Y_{CO}, %	Y_{CH4}, %	Y_{HC}, %
Ni/α-Al_2O_3	0.10	0	67.1	83.2	12.6	1.4	0.6
		5	47.5	17.6	58.4	9.3	5.4
	0.22	0	69.6	89.3	8.6	0.3	0
		5	63.5	73.0	23.3	3.0	1.1
	0.45	0	72.1	89.8	7.8	0.1	0
		5	67.7	85.4	14.2	1.6	0.2
Ni/La_2O_3-αAl_2O_3	0.10	0	69.2	88.6	8.6	0.8	0.3
		5	59.2	58.2	34.0	6.4	3.6
	0.22	0	69.5	89.0	9.2	0.3	0
		5	68.3	84.3	10.8	0.9	0.2
	0.45	0	70.6	92.7	8.3	0.0	0
		5	68.3	90.3	9.6	0.3	0.1

Table 5. Coke contents at different temperature. Reforming conditions: S/C = 12, τ = 0.22 $g_{catalyst}$ $h/g_{bio\text{-}oil}$, t = 5 h.

Catalyst	Temperature, ºC	C_c, wt%
$Ni/\alpha\text{-}Al_2O_3$	600	2.50
	700	0.30
	800	0.10
$Ni/La_2O_3\text{-}\alpha Al_2O_3$	600	1.40
	700	0.15
	800	-

Table 6. Coke contents at different space-time. Reforming conditions: S/C = 12, 700 ºC, t = 5 h.

Catalyst	Space time $g_{catalyst}$ h $(g_{bio\text{-}oil})^{-1}$	C_c, wt%
$Ni/\alpha\text{-}Al_2O_3$	0.10	1.90
	0.22	1.00
	0.45	0.25
$Ni/La_2O_3\text{-}\alpha Al_2O_3$	0.10	0.40
	0.22	0.15
	0.45	0.11

Table 7. Average particle size of Ni (in nm) for $Ni/\alpha\text{-}Al_2O_3$ and $Ni/La_2O_3\text{-}\alpha Al_2O_3$ catalysts (fresh and deactivated after 5 h of reaction) and coke contents. Reforming conditions: 700 ºC, S/C = 12, $G_{C1}HSV = 8100\ h^{-1}$.

Catalyst	fresh	deactivated	C_c, %
$Ni/\alpha\text{-}Al_2O_3$	7.4	16.6	0.25
$Ni/La_2O_3\text{-}\alpha Al_2O_3$	11.9	12.3	0.11

FIGURES

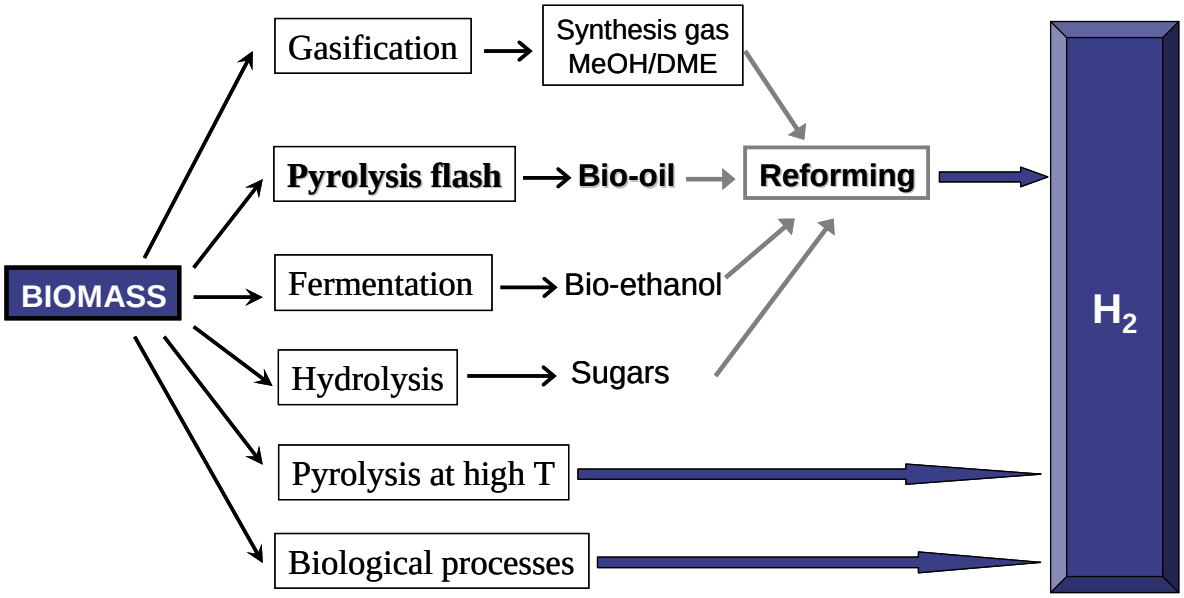

Figure 1

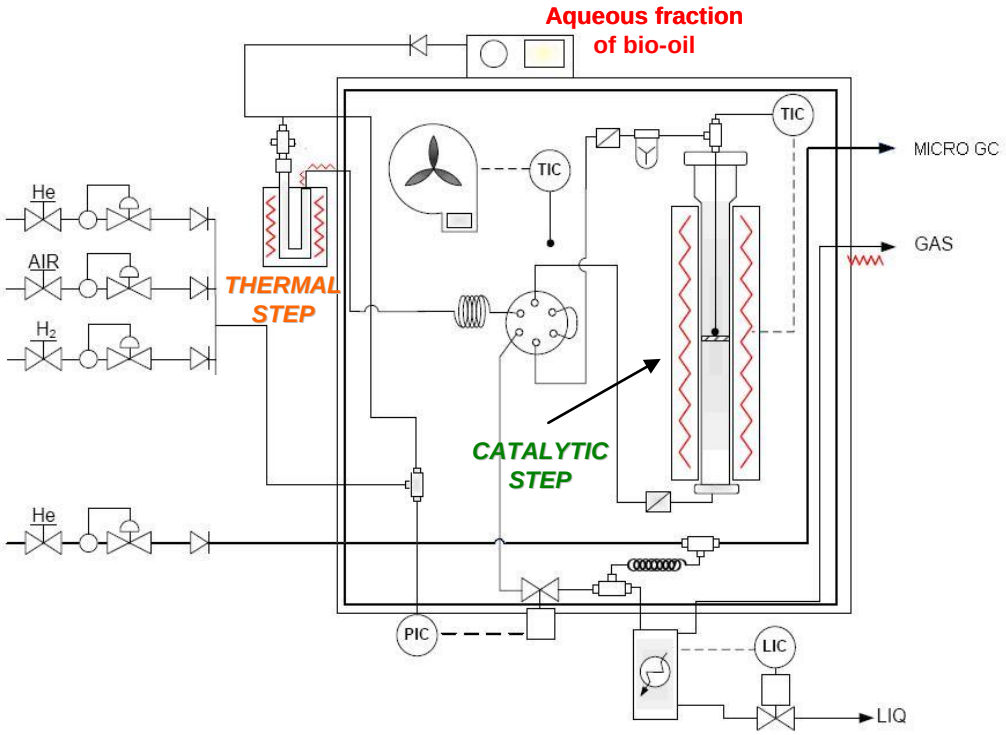
Aqueous fraction
of bio-oil
TIC
TIC
MICRO GC
GAS
He
AIR
H2
THERMAL
STEP
CATALYTIC
STEP
He
PIC
LIC
LIQ

Figure 2

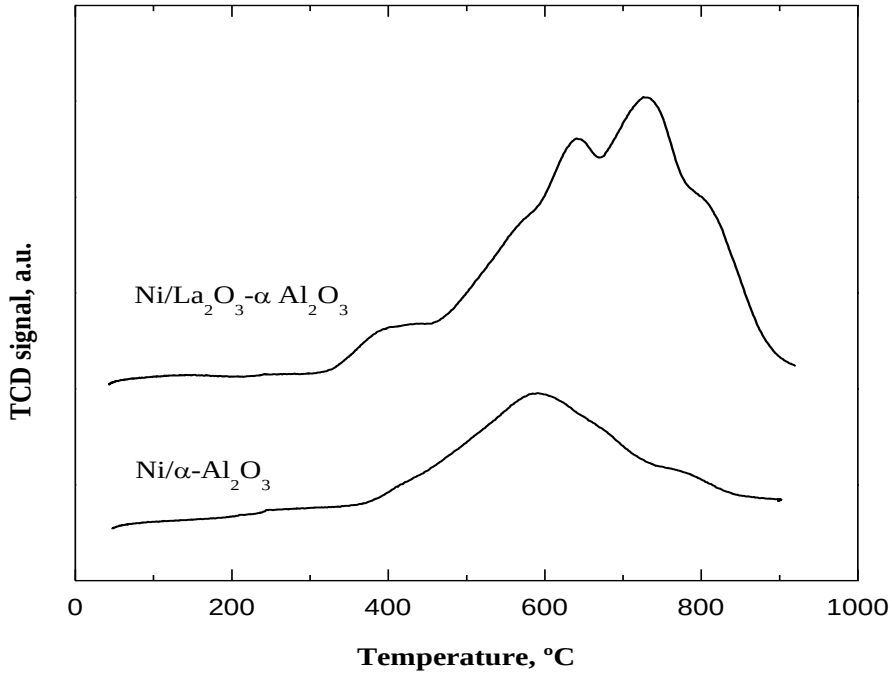
TCD signal, a.u.
Ni/La2O3-α Al2O3
Ni/α-Al2O3
0
200
400
600
800
1000
Temperature, ºC

Figure 3

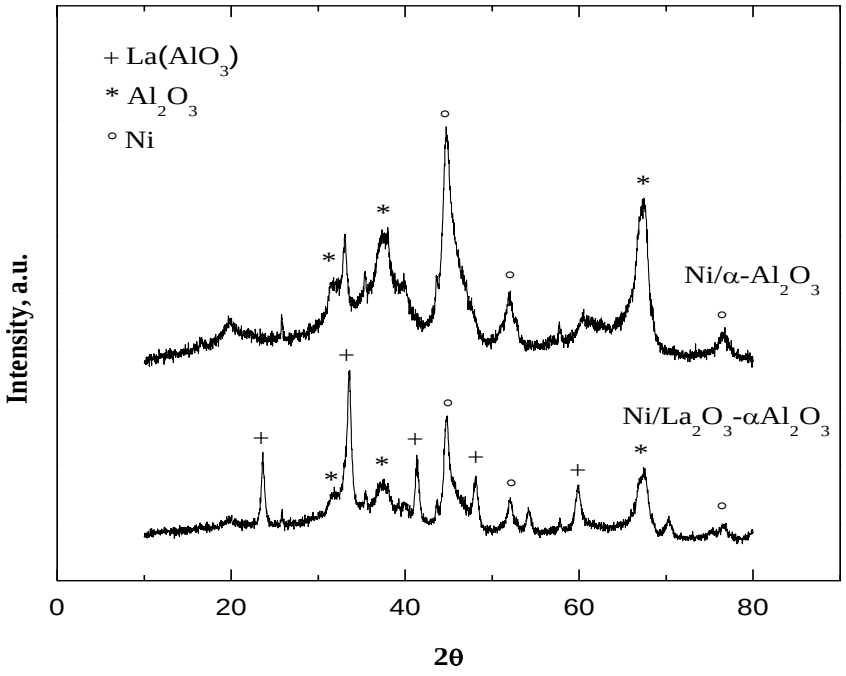
+ La(AlO3)
* Al2O3
° Ni
Ni/α-Al2O3
Ni/La2O3-αAl2O3
Intensity, a.u.
0
20
40
60
80
2θ

Figure 4

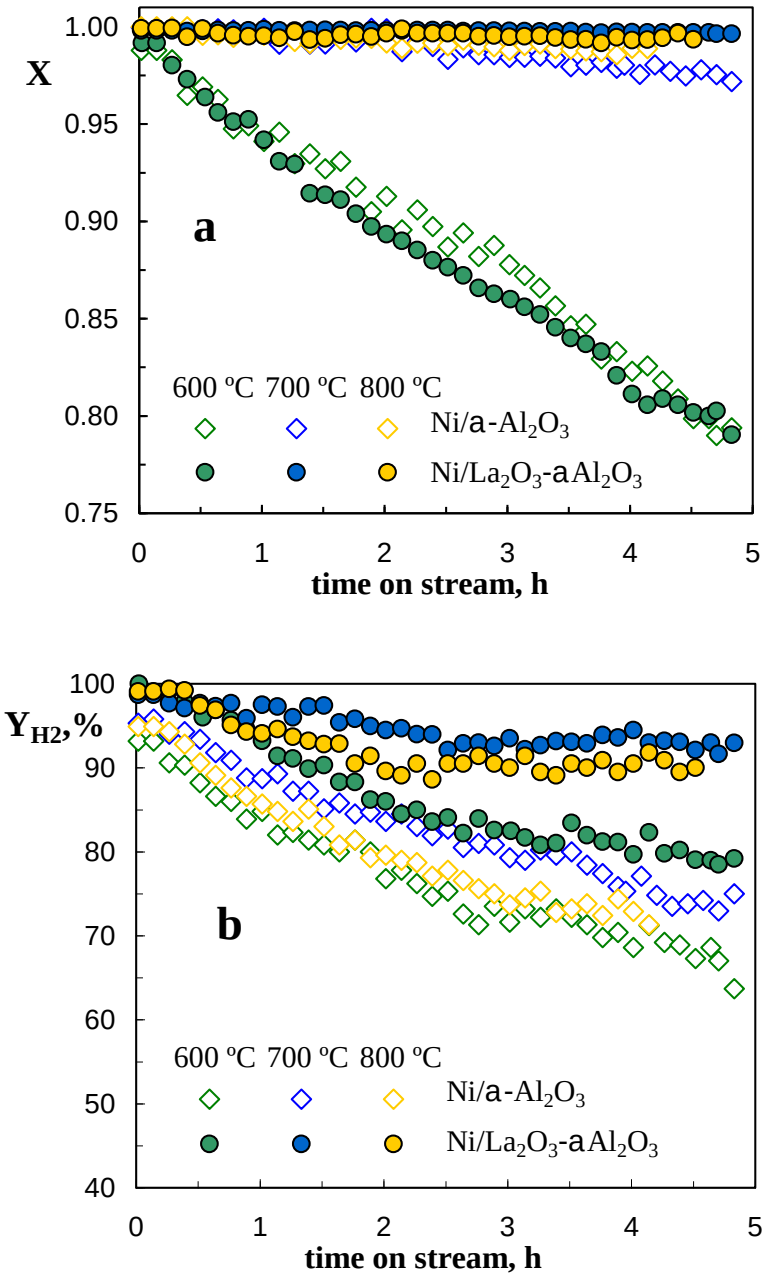
X
1.00
0.95
0.90
0.85
0.80
0.75
a
600 ºC 700 ºC 800 ºC
Ni/a-Al2O3
Ni/La2O3-aAl2O3
0
1
2
3
4
5
time on stream, h
YH2,%
100
90
80
70
60
50
40
b
600 ºC 700 ºC 800 ºC
Ni/a-Al2O3
Ni/La2O3-aAl2O3
0
1
2
3
4
5
time on stream, h

Figure 5

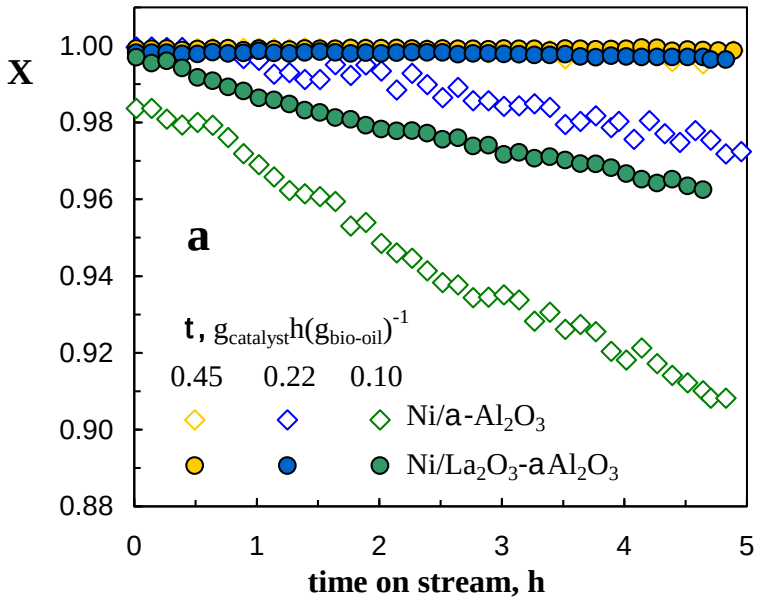
X
1.00
0.98
0.96
0.94
0.92
0.90
0.88
a
t, g_catalyst h(g_bio-oil)^-1
0.45 0.22 0.10
Ni/a-Al2O3
Ni/La2O3-aAl2O3
0 1 2 3 4 5
time on stream, h

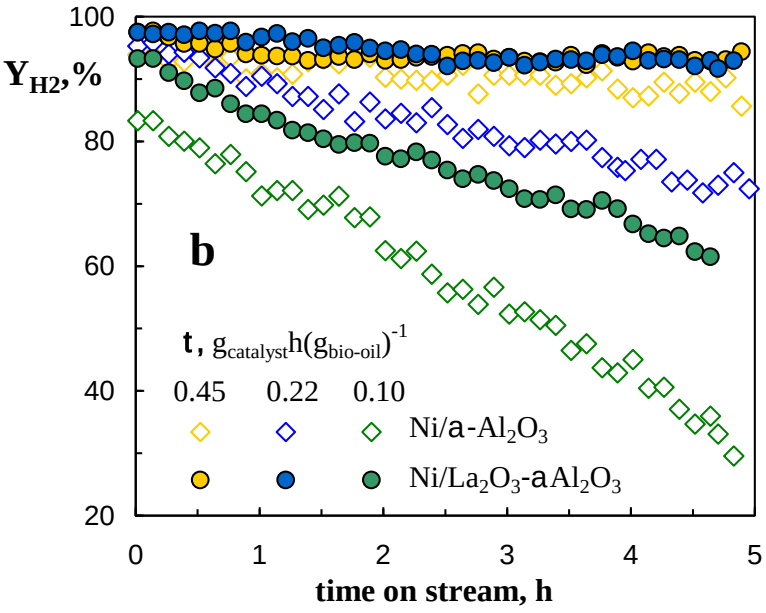
Y_H2,%
100
80
60
40
20
b
t, g_catalyst h(g_bio-oil)^-1
0.45 0.22 0.10
Ni/a-Al2O3
Ni/La2O3-aAl2O3
0 1 2 3 4 5
time on stream, h

Figure 6

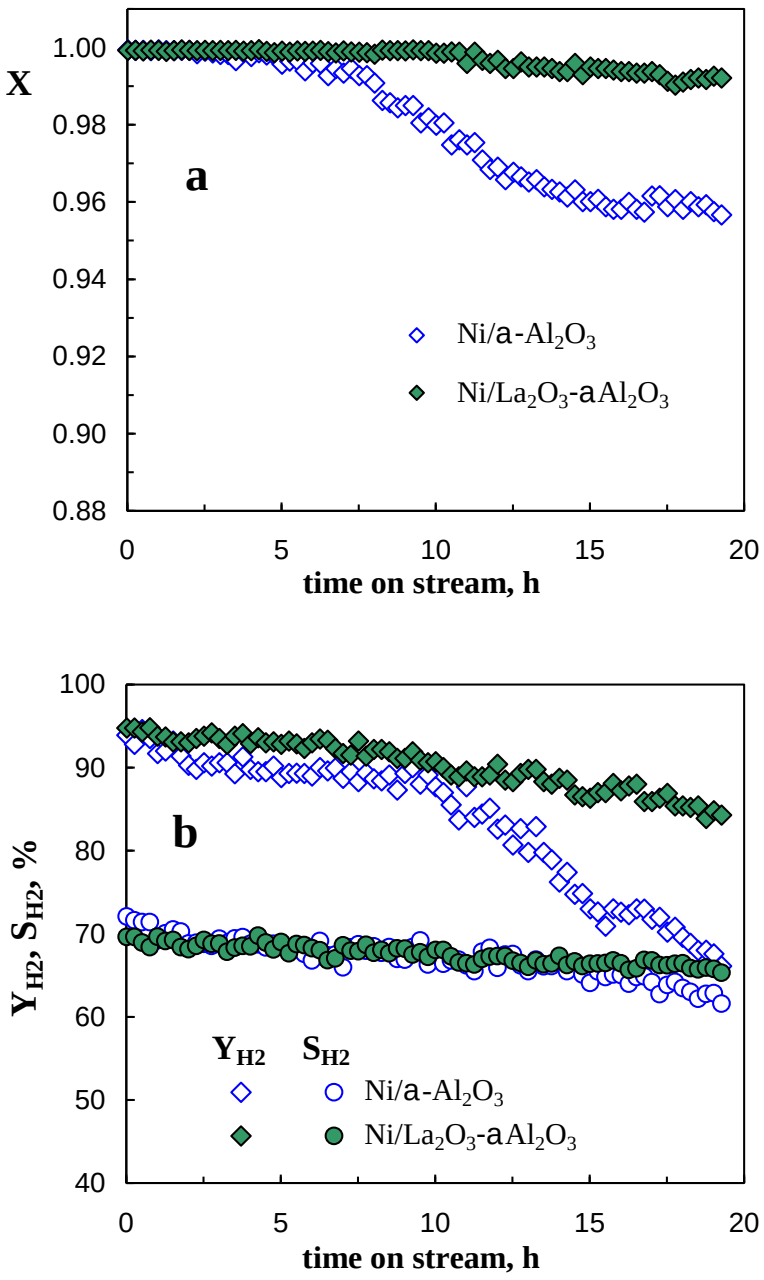
X
1.00
0.98
0.96
0.94
0.92
0.90
0.88
a
Ni/a-Al2O3
Ni/La2O3-aAl2O3
0
5
10
15
20
time on stream, h
100
90
80
70
60
50
40
YH2, SH2, %
b
YH2
SH2
Ni/a-Al2O3
Ni/La2O3-aAl2O3
0
5
10
15
20
time on stream, h

Figure 7

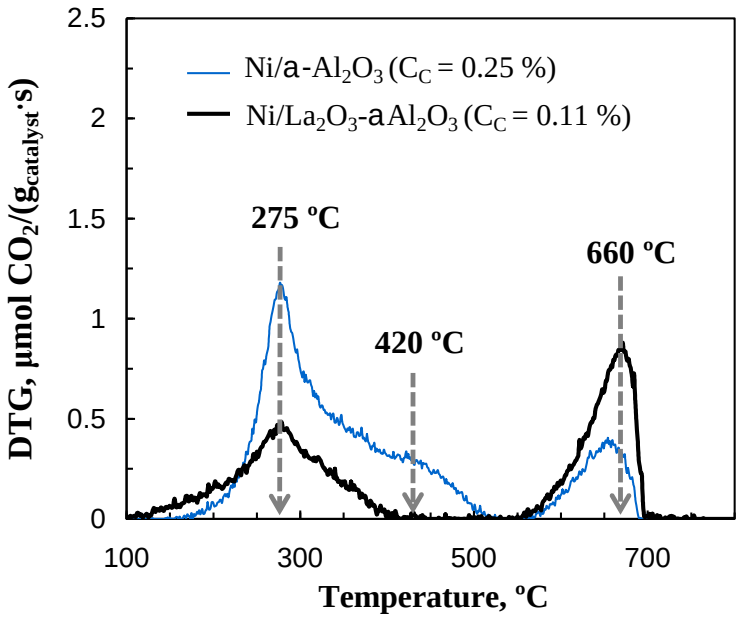
2.5
2
1.5
1
0.5
0
100
300
500
700
Ni/a-Al2O3 (CC = 0.25 %)
Ni/La2O3-aAl2O3 (CC = 0.11 %)
275 ºC
420 ºC
660 ºC
DTG, µmol CO2/(gcatalyst·s)
Temperature, ºC

Figure 8

Figure
Click here to download high resolution image

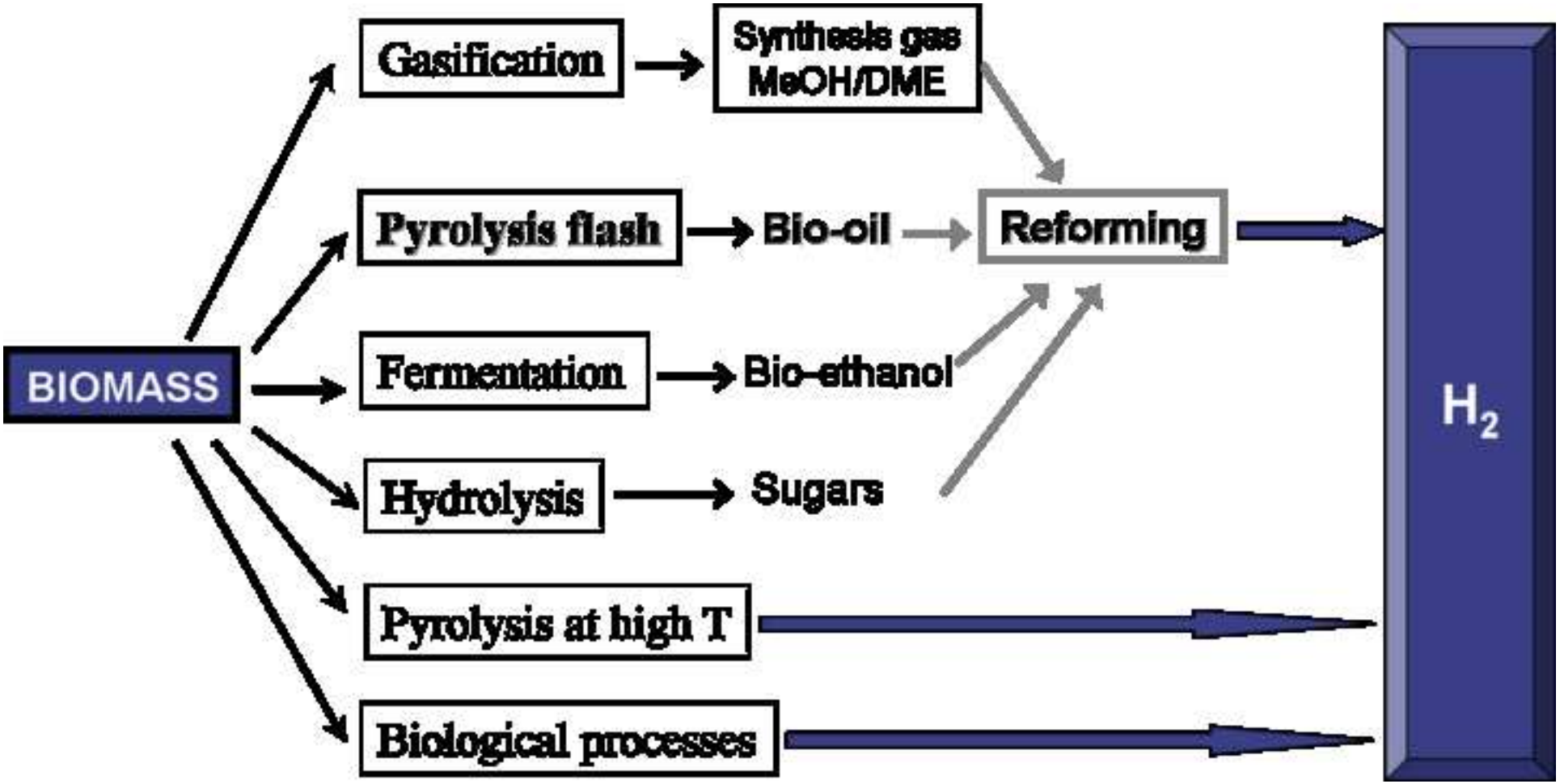

Figure

Click here to download high resolution image

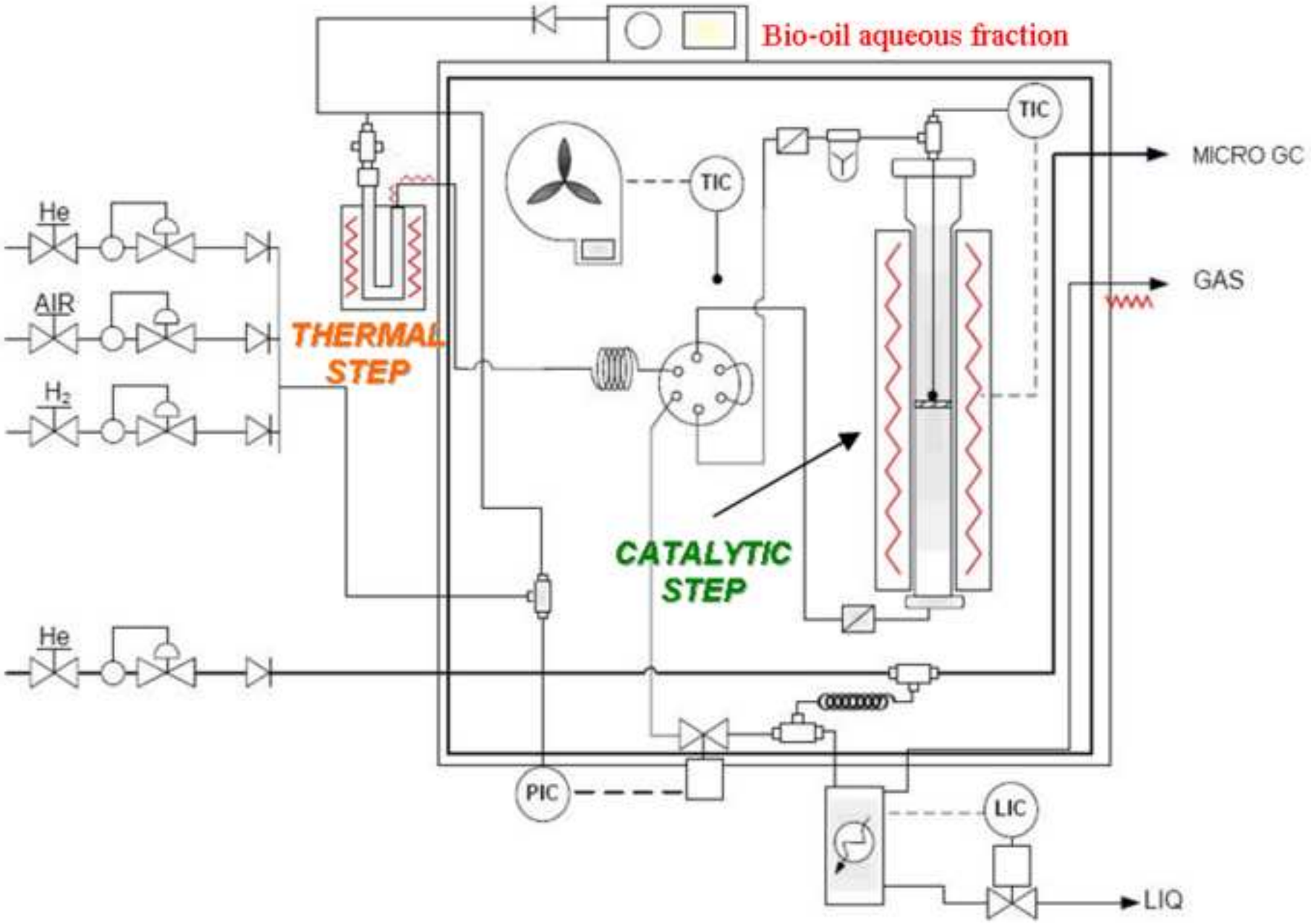

Figure

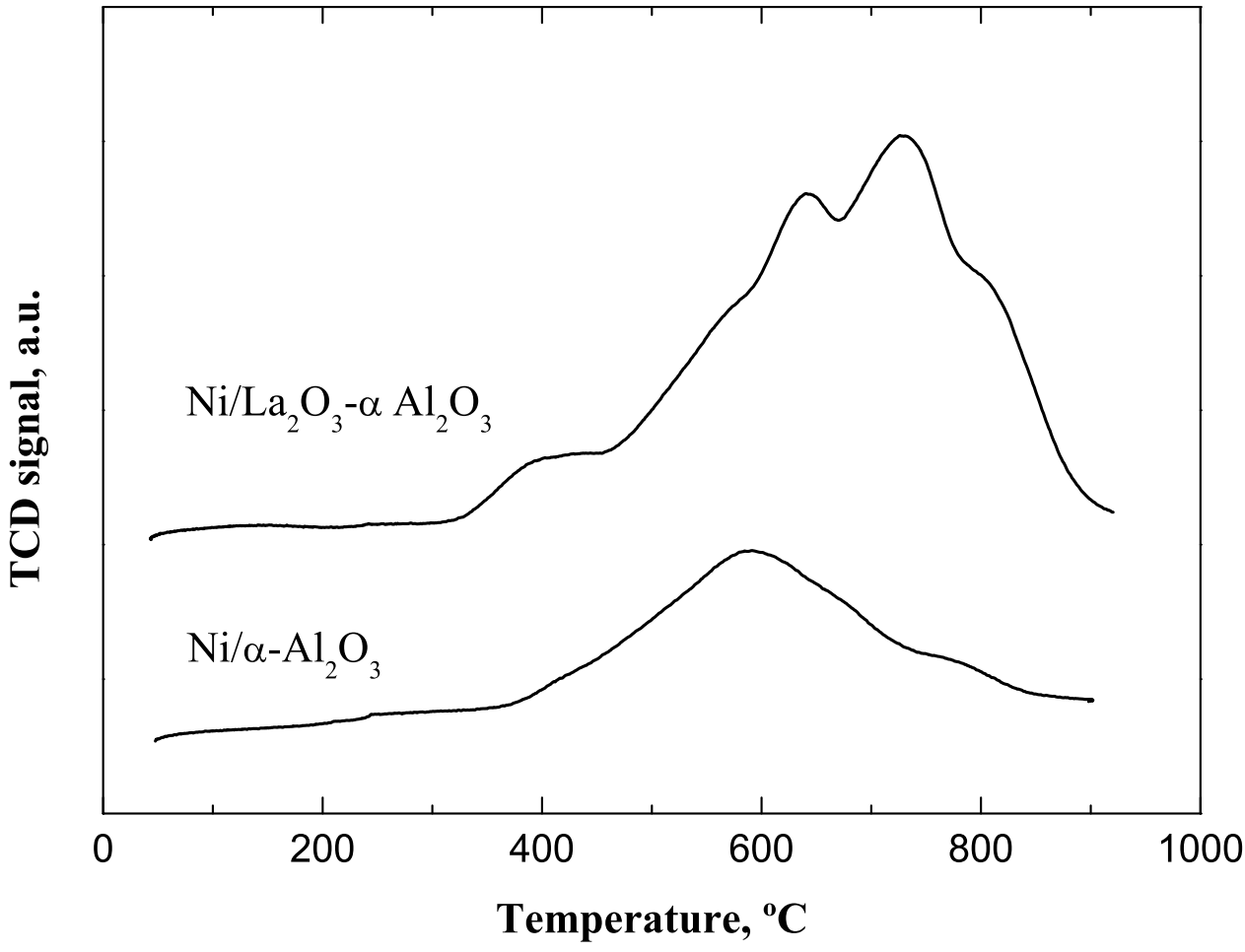
TCD signal, a.u.
Ni/La2O3-α Al2O3
Ni/α-Al2O3
0
200
400
600
800
1000
Temperature, °C

Figure

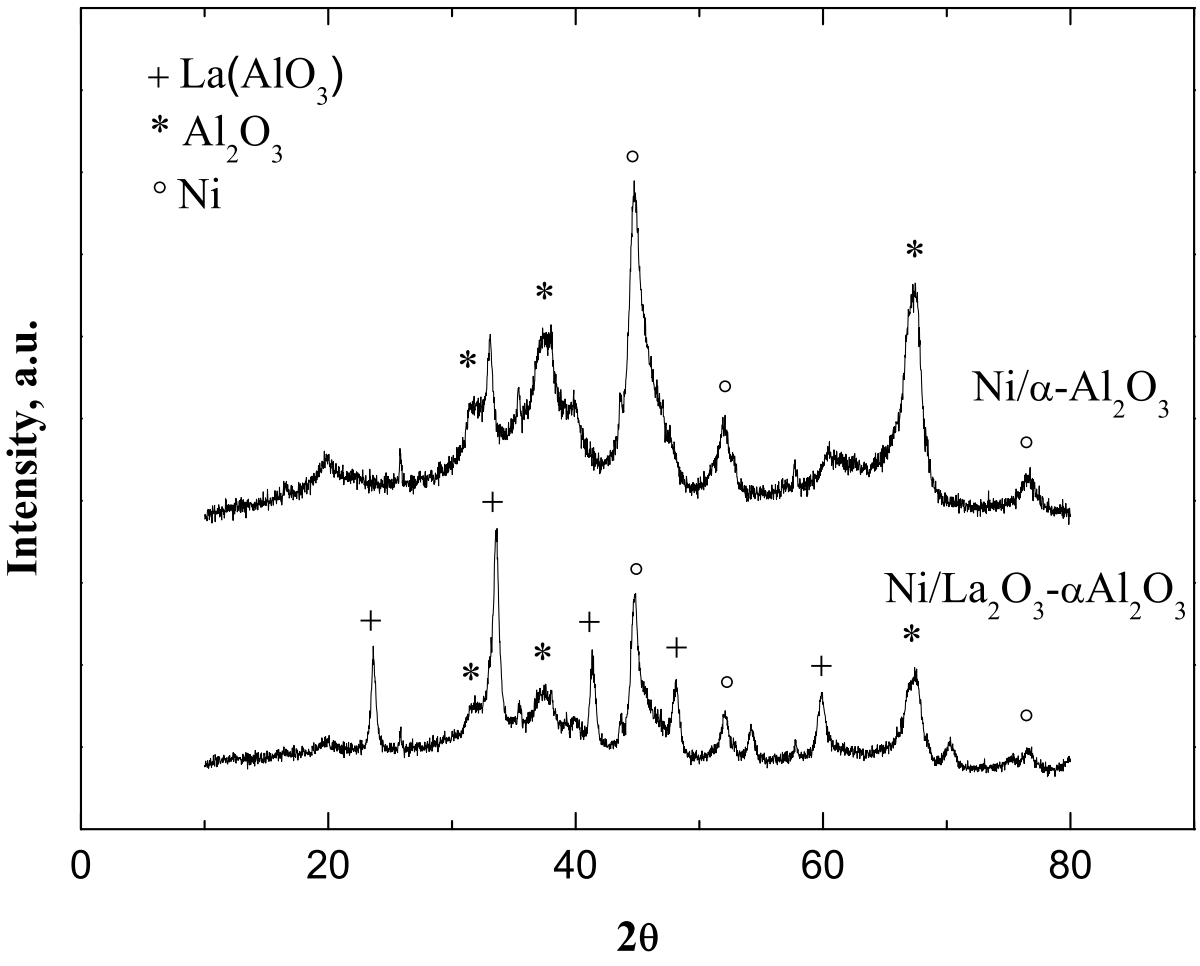
+ La(AlO3)
* Al2O3
◦ Ni
Ni/α-Al2O3
Ni/La2O3-αAl2O3
Intensity, a.u.
0
20
40
60
80
2θ

Figure

Click here to download high resolution image

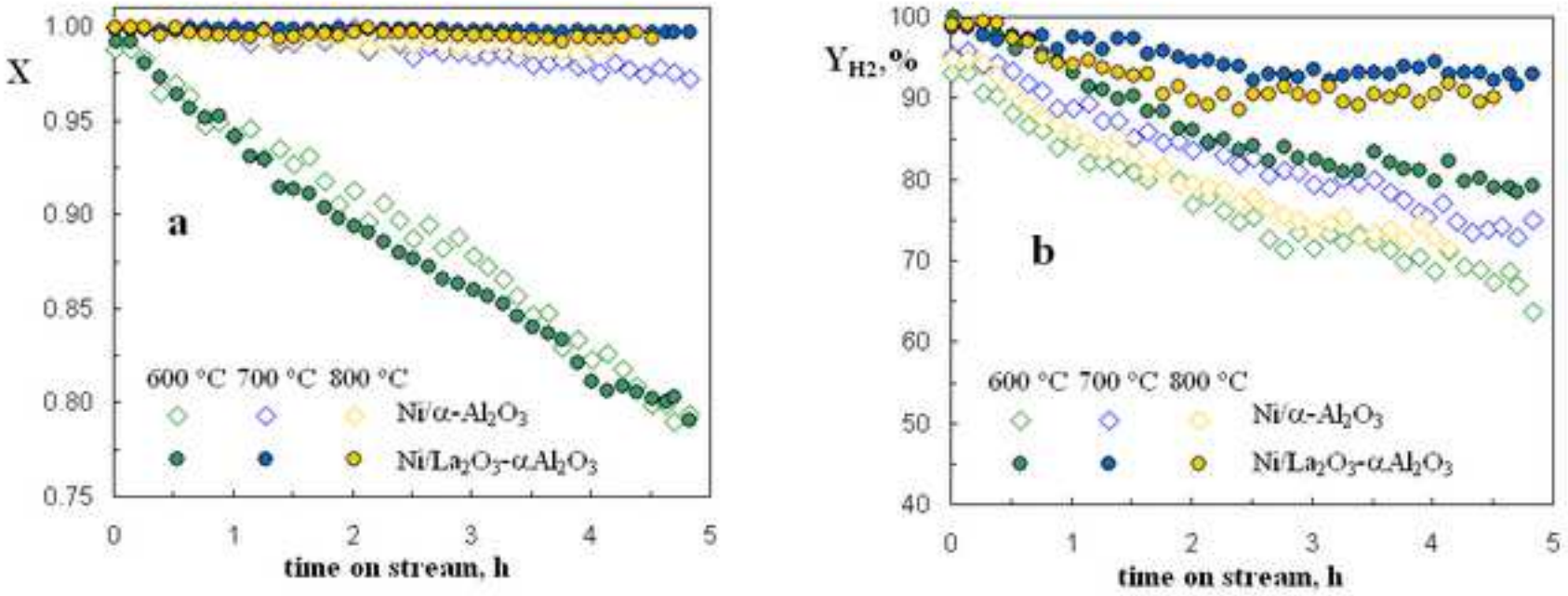

Figure

Click here to download high resolution image

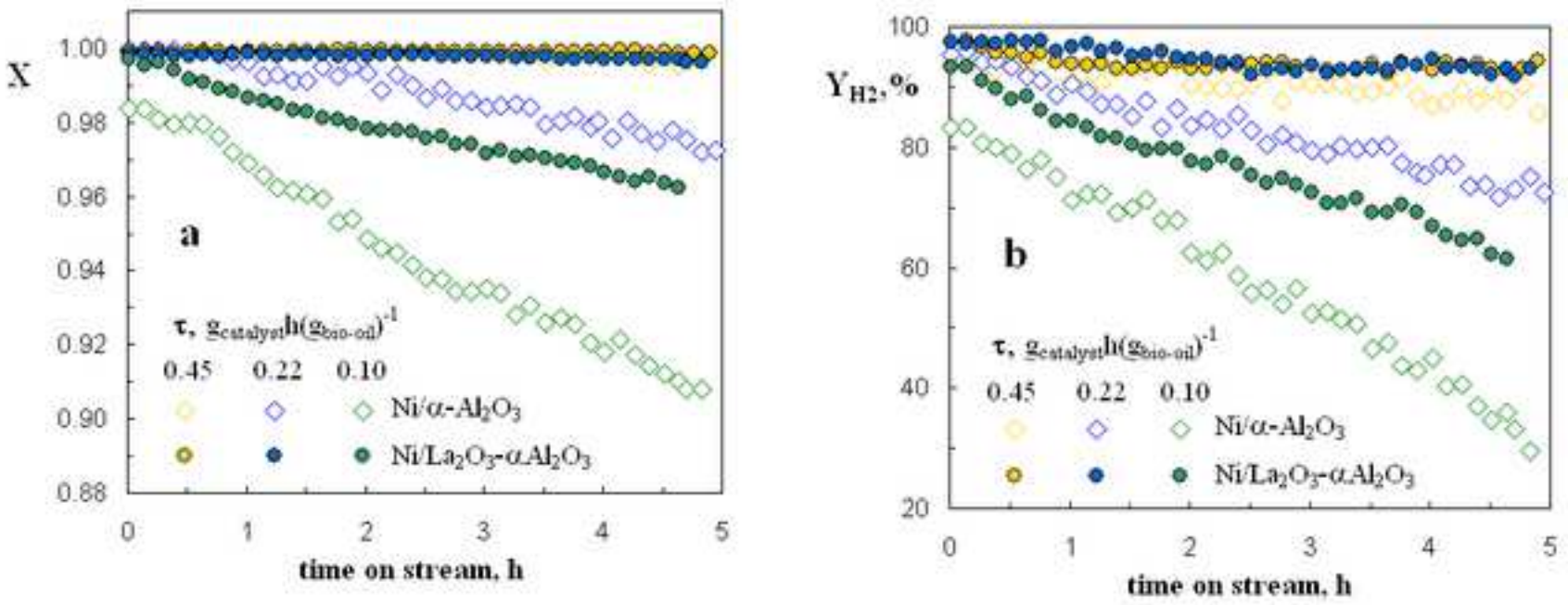

Figure

Click here to download high resolution image

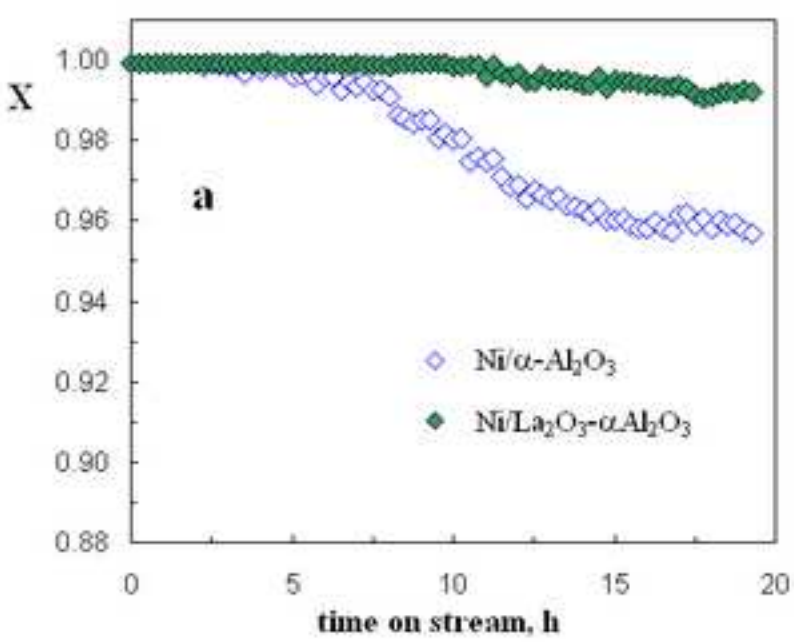

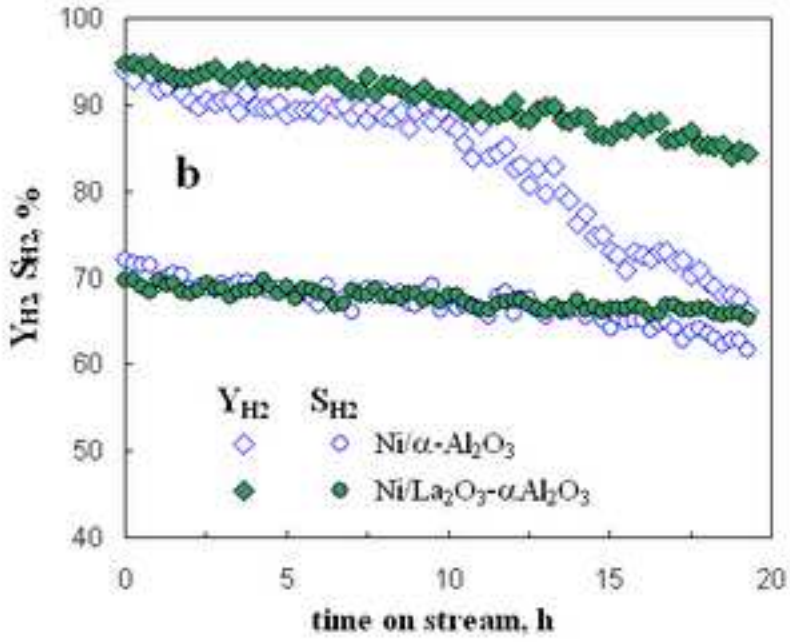

Figure
Click here to download high resolution image